Dalton Transactions

PAPER

View Article Online
View Journal | View Issue

Cite this: *Dalton Trans.*, 2015, **44**, 18596

Intramolecular C–H oxidative addition to iridium(I) triggered by trimethyl phosphite in *N,N′*-diphosphanesilanediamine complexes†‡

Vincenzo Passarelli,*[a,b] Jesús J. Pérez-Torrente[b] and Luis A. Oro[b]

Received 27th July 2015,
Accepted 22nd September 2015

DOI: 10.1039/c5dt02886h

www.rsc.org/dalton

The reaction of [Ir(SiNP)(cod)][PF_6] ([**1**][PF_6]) and of IrCl(SiNP)(cod) (**5**) (SiNP = $SiMe_2\{N(4\text{-}C_6H_4CH_3)PPh_2\}_2$) with trimethyl phosphite affords the iridium(III) derivatives of the formula $[IrHCl_x(SiNP\text{-}H)\{P(OMe)_3\}_{2-x}]^{(1-x)+}$ (x = 0, **3**$^+$; x = 1, **6**) containing the κ^3C,P,P'-coordinated SiNP-H ligand (SiNP-H = $Si(CH_2)(CH_3)\{N(4\text{-}C_6H_4CH_3)PPh_2\}_2$). The thermally unstable pentacoordinated cation $[Ir(SiNP)\{P(OMe)_3\}(cod)]^+$ (**2**$^+$) has been detected as an intermediate of the reaction and has been fully characterised in solution. Also, the mechanism of the C–H oxidative addition has been elucidated by DFT calculations showing that the square planar iridium(I) complexes of the formula $[IrCl_x(SiNP)\{P(OMe)_3\}_{2-x}]^{(1-x)+}$ (x = 0, **4**$^+$; x = 1, **7**) should be firstly obtained from **2**$^+$ and finally should undergo the C–H oxidative addition to iridium(I) *via* a concerted intramolecular mechanism. The influence of the counterion of **2**$^+$ on the outcome of the C–H oxidative addition reaction has also been investigated.

Introduction

In the last few years amino-phosphanes have attracted lots of interest due to their easy functionalisation and their ability to afford metal complexes active both in stoichiometric and catalytic reactions.[1] Motivated by the scarce number of complexes with *N,N′*-diphosphanesilanediamino ligands, we prepared the ligand $SiMe_2\{(N(4\text{-}C_6H_4CH_3)(PPh_2)\}_2$ (SiNP, Scheme 1A) and explored the synthesis and reactivity of its rhodium[2] and iridium[3] derivatives. As a result of our investigation, we reported that the κ^2P,P' coordination mode is the most frequent in the rhodium and iridium complexes prepared so far. Nevertheless, we also described the unprecedented κ^3C,P,P' coordination mode. Indeed, as a consequence of the cyclometalation reaction in the square planar complex IrCl(SiNP)(CO), the hydride derivative IrHCl(SiNP-H)(CO), containing two fused five membered IrPNSiC rings, is obtained (Scheme 1A).[3]

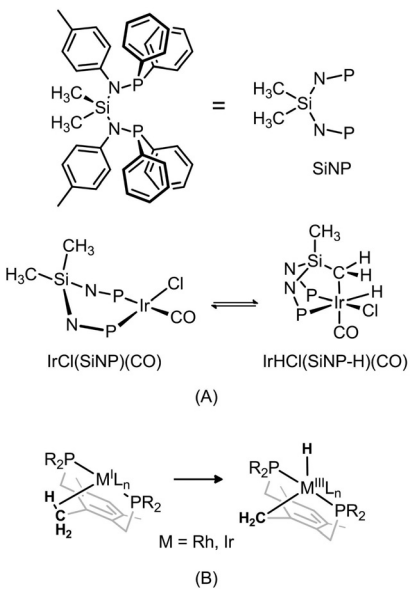

Scheme 1

Despite the large number of cyclometalation reactions involving transition metals,[4] to the best of our knowledge, the oxidative addition of a methyl C–H bond from a diphosphano ligand to rhodium or iridium has been described only for complexes containing the *trans* spanning ligand 1,3-$(CH_2P^tBu_2)$-2,4,6-$(CH_3)_3(C_6H)$.[5] In this case, as a consequence of the rigidity of the ligand backbone, the C–H is brought close to the metal centre and consequently the C–H bond activation takes place (Scheme 1B).

[a]*Centro Universitario de la Defensa, Ctra. Huesca s/n, ES-50090 Zaragoza, Spain. E-mail: passarel@unizar.es*
[b]*Departamento de Química Inorgánica, Instituto de Síntesis Química y Catálisis Homogénea (ISQCH), Universidad de Zaragoza-CSIC, C/ Pedro Cerbuna 12, ES-50009 Zaragoza, Spain*

† In honour of Prof. Guido Pampaloni, Università di Pisa (Italia), on the occasion of his 60th birthday.

‡ Electronic supplementary information (ESI) available: Selected NMR data, kinetic data and atomic coordinates of the DFT calculated structures. CCDC 1413967. For ESI and crystallographic data in CIF or other electronic format see DOI: 10.1039/c5dt02886h

Conversely, our preliminary study on the cyclometalation reaction in IrCl(SiNP)(CO) showed that the two phosphorus atoms occupy *cis* positions and that the six membered IrP_2N_2Si ring adopts a boat conformation.[3] Consequently, the flag-pole $SiCH_3$ is directed toward the iridium(I) centre allowing the oxidative addition of the $SiCH_2$–H bond to the metal centre (Scheme 1A).

On this basis we decided to study the influence of the ancillary ligands on the course and the outcome of the intramolecular C–H oxidative addition of the SiNP ligand coordinated to iridium and eventually on the structure of the resulting products. Thus we started investigating the reactivity of [Ir(SiNP)(cod)][PF_6] ([**1**][PF_6]) and IrCl(SiNP)(cod) (**5**) towards different P-donor ligands, namely triphenylphosphane, triphenyl phosphite and trimethyl phosphite. Surprisingly, when the bulkier triphenylphosphane and triphenyl phosphite are used, no reaction is observed even using excess ligand and prolonged reaction times. Reasonably, the steric hindrance of the incoming ligand prevents the coordination to the metal centre. Nevertheless, the less sterically demanding trimethyl phosphite reacts smoothly with both [Ir(SiNP)(cod)][PF_6] ([**1**][PF_6]) and IrCl(SiNP)(cod) (**5**) at room temperature. Herein, we report the synthesis and characterisation of the resulting complexes along with the elucidation of the reaction pathway.

Results and discussion

Reaction of [Ir(SiNP)(cod)][PF_6] with $P(OMe)_3$

The reaction of $[Ir(SiNP)(cod)]^+$ ($\mathbf{1}^+$) (as the hexafluorophosphate salt) with trimethyl phosphite (1 : 1 molar ratio) readily and quantitatively affords the pentacoordinated cation $[Ir(SiNP)\{P(OMe)_3\}(cod)]^+$ ($\mathbf{2}^+$). At room temperature this complex is thermally unstable in solution and readily undergoes the intramolecular oxidative addition of the $SiCH_2$–H bond (100% conversion after approx. 60 min), affording the hydride derivative $[IrH(SiNP\text{-}H)\{P(OMe)_3\}_2]^+$ ($\mathbf{3}^+$) along with equimolar quantities of $\mathbf{1}^+$ and cod (Scheme 2, path A). On this basis, the reaction between $\mathbf{1}^+$ and $P(OMe)_3$ affording $\mathbf{2}^+$ should be reversible and $\mathbf{3}^+$ should form *via* the irreversible reaction of free $P(OMe)_3$ with $\mathbf{2}^+$. As a confirmation, when the starting molar ratio $P(OMe)_3 : \mathbf{1}^+$ is 2 : 1, $\mathbf{2}^+$ readily forms and further reacts with excess $P(OMe)_3$ yielding cleanly and quantitatively $\mathbf{3}^+$ (Scheme 2, path B) and $\mathbf{1}^+$ is not observed in the final mixture (^{31}P NMR).

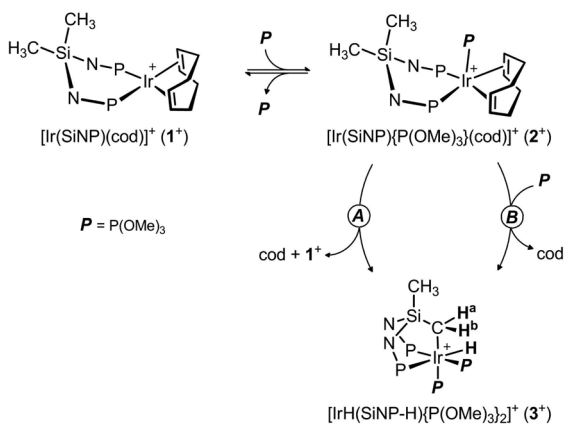

Scheme 2

Molecular structure and fluxional behaviour of [Ir(SiNP){P(OMe)$_3$}(cod)]$^+$ ($\mathbf{2}^+$) in solution. As mentioned before, the cation $[Ir(SiNP)\{P(OMe)_3\}(cod)]^+$ ($\mathbf{2}^+$) is thermally unstable and could be characterised only in CD_2Cl_2 solution at 243 K. Its $^{31}P\{^1H\}$ NMR spectrum shows one doublet for the phosphorus atoms of SiNP and one triplet for the phosphite ligand (243 K, Fig. 1A). Thus both SiNP phosphorus atoms are coordinated to iridium and the left and right semispaces at the SiNP ligand are equivalent (Fig. 2A), that is the phosphorus atoms of SiNP should be either equivalent or averaged by a fluxional process. Also, the two tolyl groups are equivalent (^1H, ^{13}C) confirming this hypothesis (*cf.* the Experimental section). Further, the ^1H NMR spectrum of $\mathbf{2}^+$ at 243 K shows two non-equivalent $SiCH_3$ groups suggesting that at that temperature the up and down semispaces at the SiNP are non-equivalent (Fig. 2A). On this basis, a variable temperature NMR study was undertaken in order to assess if $\mathbf{2}^+$ undergoes a fluxional process in solution.

At 183 K (CD_2Cl_2) the $^{31}P\{^1H\}$ NMR spectrum shows three doublets-of-doublets (Fig. 1, SiNP: δ_P = 40.2 ppm, $^2J_{PP}$ = 41.0, 36.2 Hz, P^1; δ_P = 42.3 ppm, $^2J_{PP}$ = 41.0, 5.0 Hz, P^2; $P(OMe)_3$: δ_P = 88.1 ppm, $^2J_{PP}$ = 36.2, 5.0 Hz, P^3) indicating that the two

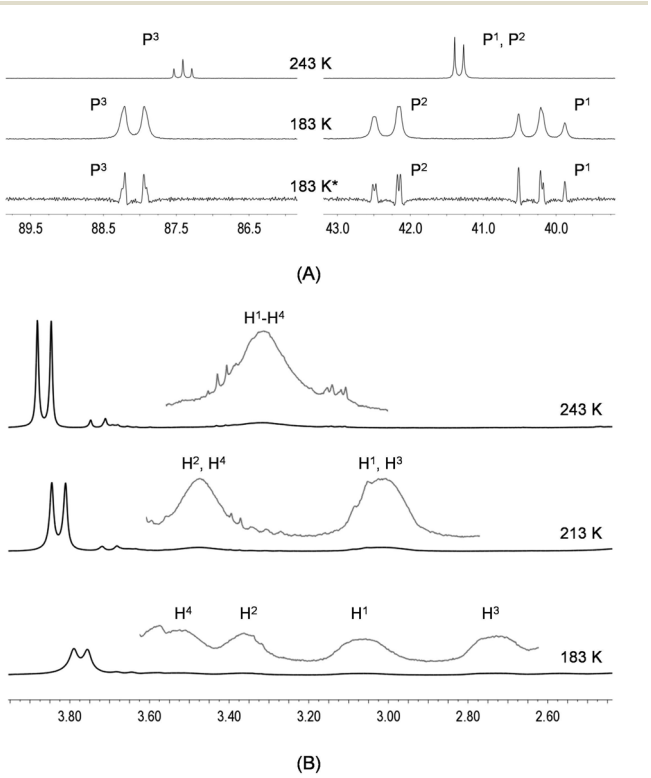

Fig. 1 Selected regions of the $^{31}P\{^1H\}$ (A) and ^1H NMR spectra (B) of $[Ir(SiNP)\{P(OMe)_3\}(cod)]^+$ ($\mathbf{2}^+$) at different temperatures (CD_2Cl_2). See Fig. 3 for the assignment. *Sine bell apodization.

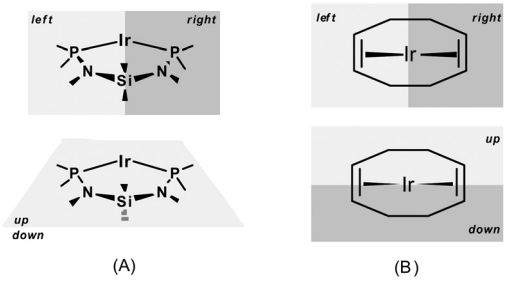

Fig. 2 Definition of the left and right and the up and down semispaces at the coordinated SiNP (A) and the coordinated cod ligands (B).

phosphorus atoms of the SiNP ligand are non-equivalent and occupy two mutually *cis* positions ($^2J_{PP}$ = 41.0).

The line shape analysis of the $^{31}P\{^1H\}$ NMR spectra of 2^+ in the range 188–228 K afforded the kinetic constants for the left–right exchange of the SiNP ligand and the activation parameters were obtained from the Eyring plot ($\Delta H^{\ddagger}$ = 53.6 ± 0.4 kJ mol^{-1}; $\Delta S^{\ddagger}$ = 71.2 ± 2.0 J mol^{-1} K^{-1}, *cf.* ESI-Table S1 and Fig. S1‡). Despite the positive $\Delta S^{\ddagger}$ value, the small value of $\Delta H^{\ddagger}$ could be considered a clue that a dissociative pathway entailing the reversible dissociation of one iridium–phosphorus bond should be ruled out. As a confirmation, such a dissociative mechanism would average the two $SiMe_2$ methyl groups, which are non-equivalent even at room temperature. Thus, reasonably the left–right exchange should be non-dissociative.

With respect to the cod ligand, one broad ^1H resonance is observed at 243 K for the olefinic hydrogen atoms (δ_{1-4} = 3.34 ppm, Fig. 1B). Thus, reasonably both the up and down and the left and right semispaces (Fig. 2B) at the cod ligand exchange. Indeed at 183 K (CD_2Cl_2) four non-equivalent $C^{sp^2}H$ hydrogen atoms are observed in the ^1H NMR spectrum (δ_4 = 3.54, δ_2 = 3.35, δ_1 = 3.06, δ_3 = 2.75 ppm, Fig. 1B) and at about 193 K the H^1 and H^3 signals and the H^2 and H^4 signals coalesce finally affording two signals at 213 K ($\delta_{2,4}$ = 3.48; $\delta_{1,3}$ = 3.03 ppm, Fig. 1B). In their turn, these two ^1H signals coalesce at about 233 K affording the above mentioned ^1H signal at 3.34 ppm (δ_{1-4}, 243 K, Fig. 1B).

In order to throw light on the overall fluxional behaviour of 2^+, its molecular structure was calculated at the DFT-B3LYP level and it was determined to be a distorted square pyramid with a SPY-5-13 [6] configuration at the metal centre (Fig. 3). In this respect, it is worth mentioning that this configuration at iridium has already been observed in the solid state structure of the cations $[Ir(PMe_3)_3(cod)]^+$ (ref. 7a) and $[Ir(PTA)_3(cod)]^+$ (ref. 7b) (PTA = 1,3,5-triaza-7-phosphaadamantane).

The presence of the apical trimethyl phosphite ligand makes non-equivalent the up and down semispaces at both the cod and the SiNP ligands and the distorted conformation of the IrP_2N_2Si ring should be responsible for the left–right non-equivalence at both the cod and SiNP ligands at 183 K. In support of the proposed SPY-5-13 structure, selected experimental and calculated NMR data are given in the caption of Fig. 3.

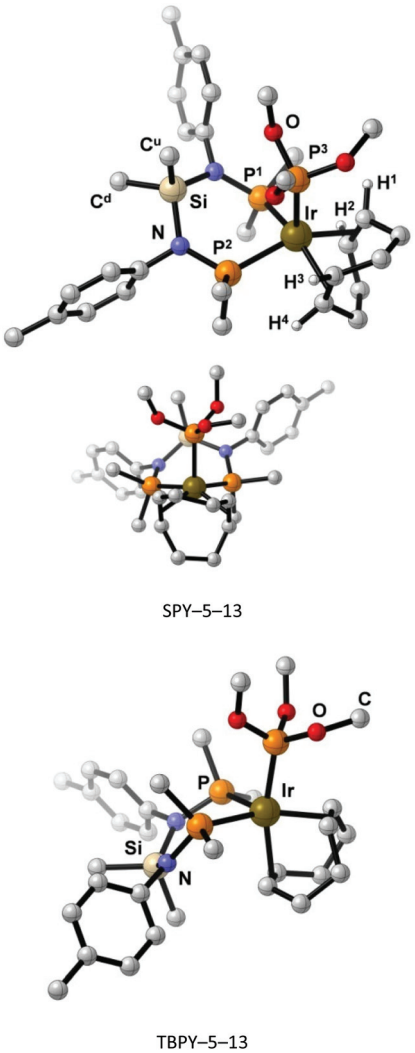

Fig. 3 Views of the DFT-calculated SPY-5-13 and TBPY-5-13 structures for $[Ir(SiNP)\{P(OMe)_3\}(cod)]^+$ (2^+). Most hydrogen atoms are omitted and only *ipso* carbon atoms of the PPh groups are shown for clarity. Selected experimental (normal type, 183 K, CD_2Cl_2) and calculated data for the SPY-5-13 structure (italic type) are in the order: δ_P = 88.1 (*87.8*, P^3), 42.3 (*43.3*, P^2), 40.2 (*37.9*, P^1); δ_H = 3.54 (*3.56*, H^4), 3.35 (*3.39*, H^2), 3.06 (*3.01*, H^1), 2.75 (*1.90*, H^3), 1.11 (*1.06*, SiC^uH_3), −0.67 (*−0.65*, SiC^dH_3).

On this basis, the non-dissociative process claimed before for the left–right exchange at the SiNP ligand should be the conformational equilibrium as shown in Scheme 3A. Further, this process exchanges also the left–right semispaces at the cod ligand and therefore should account for the coalescence of the ^1H signals at 3.54 (H^4) and 3.35 ppm (H^2) and at 3.06 (H^1) and 2.75 ppm (H^3) observed at 193 K, as well.

When dealing with the coalescence observed at about 233 K (*vide supra*), also the TBPY-5-13 [6] structure (Fig. 3) was found to be a minimum energy structure at +28.9 kJ mol^{-1} (free energy) with respect to the SPY-5-13 structure. In this regard, it should be noted that the TBPY-5-13 configuration at iridium has already been described in the solid state structure of several cations of the general formula $[Ir(P\text{-donor})_3(cod)]^+$.[7a,8]

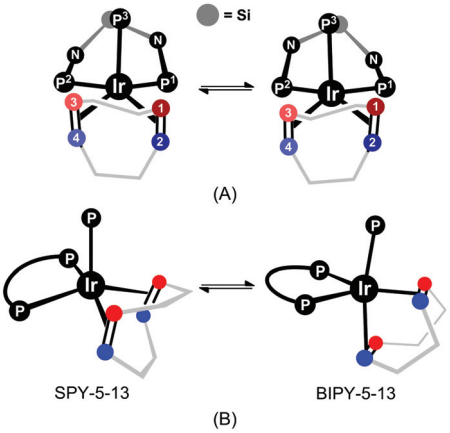

Scheme 3 Left–right (A) and up–down (B) exchange at the cod ligand of $[Ir(SiNP)\{P(OMe)_3\}(cod)]^+$ ($\mathbf{2}^+$).

Given that the TBPY-5-13 structure features equivalent up and down semispaces at the cod ligand, the equilibrium SPY-5-13 ⇄ TBPY-5-13 shown in Scheme 3B exchanges the up and down semispaces at the cod ligand in the SPY-5-13 structure and thus should account for the coalescence of the ^{1}H signals at 3.48 ($\delta_{2,4}$) and 3.03 ppm ($\delta_{1,3}$) (Fig. 1B). As a confirmation, the kinetic constants of the up–down exchange process for the cod ligand were calculated from the ^{1}H–^{1}H EXSY spectra in the range 203–223 K, and the activation parameters obtained from the Eyring plot validate the proposed concerted exchange mechanism ($\Delta H^{\ddagger}$ = 42.7 ± 1.7 kJ mol^{-1}; $\Delta S^{\ddagger}$ = 19.6 ± 7.1 J mol^{-1} K^{-1}, *cf.* ESI-Table S2 and Fig. S2‡).

For the sake of comparison, it is worth mentioning that the related carbonyl derivative[3] $[Ir(SiNP)(CO)(cod)]^+$ exhibits a distinct solution molecular structure (*vide infra*) and a different fluxional behaviour thus indicating a subtle influence of the ancillary ligand L on the structure of the pentacoordinated $[Ir(SiNP)(L)(cod)]^+$ cations.

Molecular structure of $[IrH(SiNP\text{-}H)\{P(OMe)_3\}_2]^+$ ($\mathbf{3}^+$). Single crystals of $[IrH(SiNP\text{-}H)\{P(OMe)_3\}_2][PF_6]$ ([**3**][PF_6]) were obtained and the solid state structure determination was carried out. The molecular structure of cation $\mathbf{3}^+$ (Fig. 4) shows the iridium centre in an octahedral environment in which the deprotonated SiNP-H ligand displays a κ^3*C,P,P′* coordination mode with a facial arrangement at the metal centre (C(11)–Ir(1)–P(1), 82.72(10); C(11)–Ir(1)–P(2), 84.51(9); P(1)–Ir(1)–P(2), 96.02(3)°) (Table 1).

The coordination sphere is completed by two κ*P*-phosphite ligands, one *trans* (P(3)–Ir(1)–C(11), 171.33(10)°) and the other *cis* (P(4)–Ir(1)–C(11), 88.01(9)°) to the carbon atom C(11) of the deprotonated SiNP-H ligand. The hydride ligand occupies the remaining coordination site *cis* to P(2) and P(4) and *trans* to P(1). The carbon–iridium and phosphorus–iridium bond lengths are in the range observed for related iridium complexes[9] and the silicon–carbon bond lengths are similar to those reported for $Ir(SiNP\text{-}H)(CO)_2$ (1.830(4), 1.842(4) Å)[3] and $RhCl_2(C_3H_5)(SiNP)$ (1.839(7); 1.854(6) Å).[2] Also, the

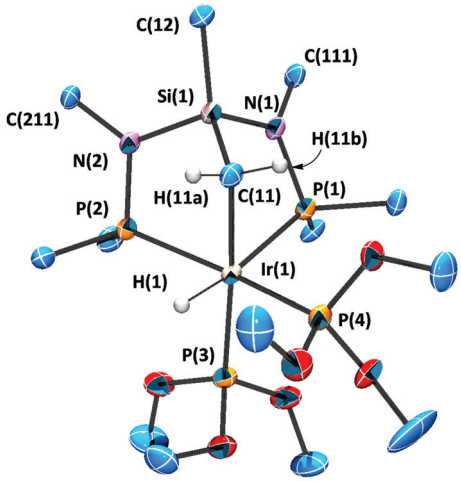

Fig. 4 ORTEP view of the cation $[IrH(SiNP\text{-}H)\{(P(OMe)_3\}_2]^+$ ($\mathbf{3}^+$) in [**3**][PF_6] with the numbering scheme adopted. Ellipsoids are at the 50% of probability. For clarity only *ipso* carbon atoms are shown and most hydrogen atoms are omitted.

Table 1 Selected angles (°) and bond lengths (Å) for $[IrH(SiNP\text{-}H)\{(P(OMe)_3\}_2][PF_6]$ ([**3**][PF_6])

C(11)–Si(1)	1.818(4)	C(11)–Ir(1)–P(2)	84.51(9)
C(11)–Ir(1)	2.196(4)	P(3)–Ir(1)–P(2)	96.69(4)
C(12)–Si(1)	1.847(4)	P(4)–Ir(1)–P(2)	165.30(4)
N(1)–P(1)	1.693(3)	P(1)–Ir(1)–P(2)	96.02(3)
N(1)–Si(1)	1.763(3)	N(1)–Si(1)–N(2)	110.67(15)
N(2)–P(2)	1.685(3)	N(1)–Si(1)–C(11)	104.35(16)
N(2)–Si(1)	1.768(3)	N(2)–Si(1)–C(11)	102.62(16)
P(1)–Ir(1)	2.3876(10)	N(1)–Si(1)–C(12)	108.82(16)
P(2)–Ir(1)	2.3909(9)	N(2)–Si(1)–C(12)	106.75(16)
P(3)–Ir(1)	2.2529(10)	C(11)–Si(1)–C(12)	123.27(17)
P(4)–Ir(1)	2.2653(10)	Si(1)–C(11)–Ir(1)	100.85(16)
C(11)–Ir(1)–P(3)	171.33(10)	C(111)–N(1)–P(1)	125.2(2)
C(11)–Ir(1)–P(4)	88.01(9)	C(111)–N(1)–Si(1)	120.6(2)
P(3)–Ir(1)–P(4)	88.86(4)	P(1)–N(1)–Si(1)	114.20(17)
C(11)–Ir(1)–P(1)	82.72(10)	C(211)–N(2)–P(2)	124.7(2)
P(3)–Ir(1)–P(1)	105.64(4)	C(211)–N(2)–Si(1)	120.7(2)
P(4)–Ir(1)–P(1)	95.56(3)	P(2)–N(2)–Si(1)	113.16(16)

C(11)–Si(1)–C(12) angle (123.27(17)°) is similar to that observed in $Ir(SiNP\text{-}H)(CO)_2$ (120.59(17)°)[3] and significantly wider than that reported for $RhCl_2(C_3H_5)(SiNP)$ (108.1(3)°),[2] reasonably as a consequence of the formation of the Ir–CH_2Si bond which forces the C(11)–Si(1)–C(12) angle to open up. Additionally, the P(1)–Ir(1)–P(2) angle is smaller in $\mathbf{2}^+$ (96.02(3)°) than in $Ir(SiNP\text{-}H)(CO)_2$ (106.61(7)°) as a consequence of the different coordination polyhedra at the metal centre.

The solid state structure of $\mathbf{3}^+$ should be preserved in solution. Indeed its ^{1}H NMR spectrum clearly indicates the presence of the hydride ligand (δ_H = −12.0 ppm) with three phosphorus atoms in the *cis* positions ($^2J_{HP}$ = 18.0 Hz) and one in the *trans* position ($^2J_{HP}$ = 128.2 Hz). Moreover the $^{31}P\{^1H\}$ NMR spectrum shows a AMXY system corresponding to four phosphorus atoms with a sawhorse-like arrangement

at the metal centre (*cf.* the Experimental section and ESI-Fig. S3‡).

As far as the $IrCH_2$ moiety is concerned, its $^{13}C\{^1H\}$ signal is a doublet at −26.2 ppm ($^2J_{CP}$ = 64.6 Hz) in agreement with the presence of a phosphorus atom in the *trans* position. In addition, relevant to the elucidation of the solution structure of $\mathbf{3}^+$, two non-equivalent methylene hydrogen atoms are observed (0.36 ppm, H^a, and 0.68 ppm, H^b, Scheme 2) and their $^1H\{^{31}P\}$ signals are a doublet (H^b, $^2J_{HH}$ = 12.3 Hz) and a doublet-of-doublets (H^a, $^2J_{HH}$ = 12.3 Hz, $^3J_{HH}$ = 2.4 Hz, *cf.* ESI-Fig. S3‡).§ These patterns indicate that the H–Ir–CH_2 fragment features a locked conformation similar to that observed in the solid state.¶

Mechanism of the formation of $[IrH(SiNP\text{-}H)\{P(OMe)_3\}_2]^+$ ($\mathbf{3}^+$). In order to elucidate the pathway leading to $[IrH(SiNP\text{-}H)\{P(OMe)_3\}_2]^+$ ($\mathbf{3}^+$), a solution of $[Ir(SiNP)\{P(OMe)_3\}(cod)]^+$ ($\mathbf{2}^+$) initially at 243 K was allowed to warm up to room temperature and the evolution of the mixture was monitored by $^{31}P\{^1H\}$ NMR spectroscopy, showing that $\mathbf{3}^+$ is formed in a clean and direct way, and no intermediates are detected. Based on this observation, the energy profile for the reaction $\mathbf{2}^+ + P(OMe)_3 \rightarrow \mathbf{3}^+ + cod$ was calculated at the DFT-B3LYP level (Fig. 5A). The square planar iridium(I) cation $[Ir(SiNP)\{P(OMe)_3\}_2]^+$ ($\mathbf{4}^+$) should form as an intermediate from the substitution of the cod ligand of $\mathbf{2}^+$ by $P(OMe)_3$ (Scheme 4A). In this respect, it should be noted that square planar cations of the general formula $[Ir(P\text{-donor})_4]^+$ have already been structurally characterised in the solid state.[10]

Relevant to the outcome of the reaction, the boat conformation of the IrP_2N_2Si ring in $\mathbf{4}^+$ directs the flag-pole $SiCH_3$ group towards the metal centre. In the following step, the oxidative addition of the C–H bond should take place *via* a concerted mechanism in which the $SiCH_3$ group approaches the metal centre, and in a synchronous way the C–H bond cleaves, the Ir–H and Ir–CH_2 bonds form, and one trimethyl phosphito ligand shifts from the equatorial plane of $[Ir(SiNP)\{P(OMe)_3\}_2]^+$ ($\mathbf{4}^+$) to the final axial position in $\mathbf{3}^+$ (see **TS_4⁺_3⁺**, Fig. 5A and C).

For the sake of comparison, Scheme 4B shows the already described reactions leading to IrHCl(SiNP-H)(CO),[3] and Fig. 5B displays the corresponding energy profile calculated herein at the DFT-B3LYP level. Interestingly the two transition states **TS_CO** and **TS_4⁺_3⁺** feature similar conformations of the SiNP ligand although subtle differences are observed in the C···H, Ir···H and Ir···CH_2 lengths and the C–Si–C angle (Fig. 5C). Indeed, shorter Ir···H and Ir···CH_2 and a longer C···H length along with a slightly wider C–Si–C angle are observed in **TS_CO** suggesting that the transition state **TS_CO** is later than **TS_4⁺_3⁺**.

As a concluding remark, it is worth mentioning that electronic factors should be mainly responsible for the lower calculated barrier for the oxidative addition to $Ir(SiNP)\{P(OMe)_3\}_2^+$ ($\mathbf{4}^+$) with

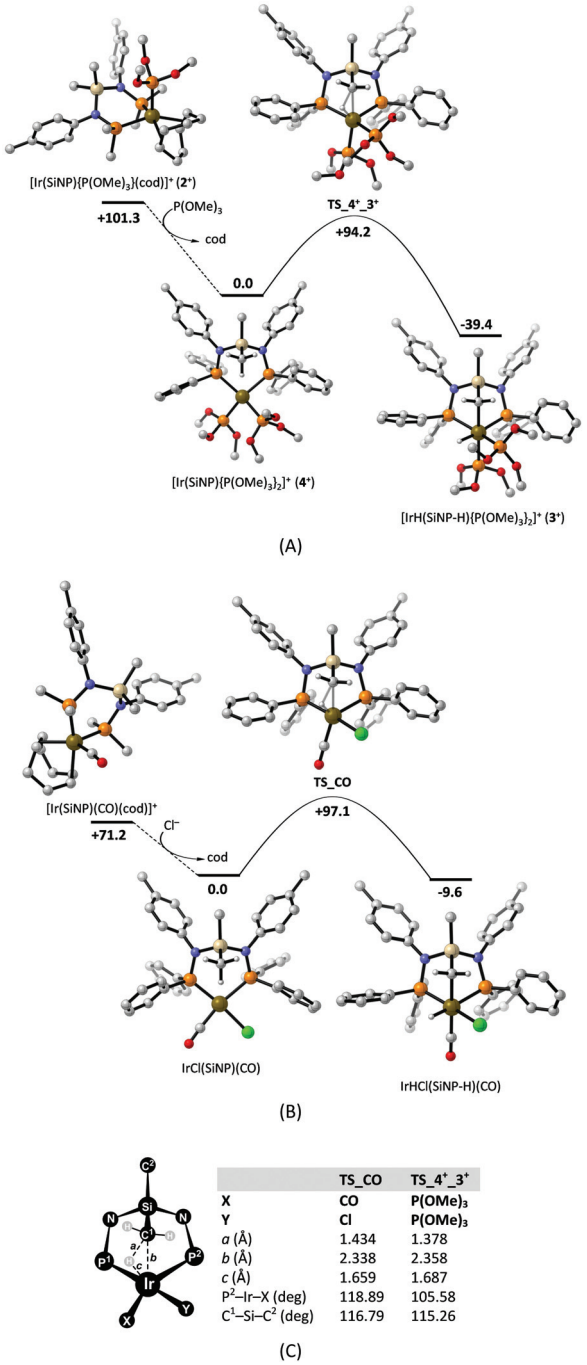

	TS_CO	TS_4⁺_3⁺
X	CO	$P(OMe)_3$
Y	Cl	$P(OMe)_3$
a (Å)	1.434	1.378
b (Å)	2.338	2.358
c (Å)	1.659	1.687
P^2–Ir–X (deg)	118.89	105.58
C^1–Si–C^2 (deg)	116.79	115.26

(C)

Fig. 5 Energy profiles (*G*, kJ mol^{-1}) of (A) the reaction $\mathbf{2}^+ + P(OMe)_3 \rightarrow \mathbf{3}^+ + cod$, and (B) the reaction $[Ir(SiNP)(CO)(cod)]^+ + Cl^- \rightarrow IrHCl(SiNP\text{-}H)(CO) + cod$. (C) Selected interatomic distances and angles for **TS_CO** and **TS_4⁺_3⁺**. The molecular structures shown have been optimised at the DFT-B3LYP level in CH_2Cl_2 at 298 K and 1 atm. Most hydrogen atoms are omitted and only *ipso* carbon atoms in $\mathbf{2}^+$ and $[Ir(SiNP)(CO)(cod)]^+$ are shown for clarity.

§ The $\Delta\nu_{1/2}$ of the $^1H\{^{31}P\}$ signal of the hydride is about 5.7 Hz, thus preventing the direct observation of the scalar coupling constant between the hydride and the H^a hydrogen ($^3J_{HH}$ = 2.4 Hz, *cf.* ESI-Fig. S3‡).

¶ As a confirmation of this hypothesis, it is worth mentioning that the Karplus curve for the H–X–Y–H system generally shows a local maximum at the dihedral angle H–X–Y–H of 0° and a local minimum, *i.e.* $^3J_{HH}$ close to 0 Hz, at near 90° (see M. J. Minch, *Concepts in Magn. Reson.*, 1994, **6**, 41). Accordingly, the solid state H(1)–Ir(1)–C(11)–H(11a) and H(1)–Ir(1)–C(11)–H(11b) dihedral angles are −8.2 and 114.7°, respectively, and the DFT-calculated structure for $\mathbf{3}^+$ features H–Ir–C–H^x angles of −13.1 (*x* = a) and 107.0° (*x* = b), respectively.

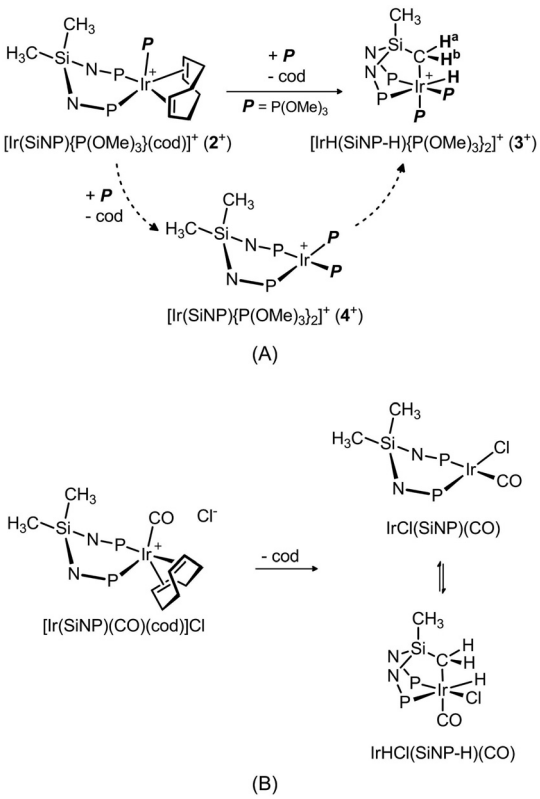

Scheme 4 (A) Proposed mechanism for the transformation of 2^+ into 3^+. (B) Formation of IrHCl(SiNP-H)(CO).[3]

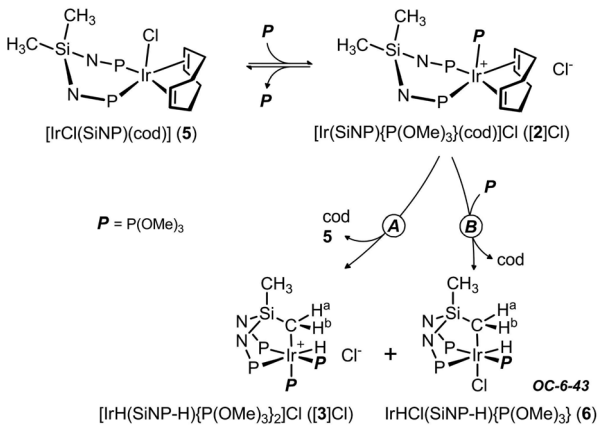

Scheme 5

respect to IrCl(SiNP)(CO) and for the consequent observed longer reaction time (6 h)[3] for the formation of IrHCl(SiNP-H)(CO). Indeed, if the steric congestion at iridium was decisive the oxidative addition of the $SiCH_2$–H bond should be faster in the less hindered IrCl(SiNP)(CO) than in $Ir(SiNP)\{P(OMe)_3\}_2^+$ (4^+). Moreover, the stronger π-acceptor character of CO when compared with that of $P(OMe)_3$,[11] and the consequent calculated atomic charges at iridium (−0.020*e* in IrCl(SiNP)(CO); −0.130*e* in 4^+) fairly parallels the observed faster C–H oxidative addition in 4^+.‖

Reaction of IrCl(SiNP)(cod) with $P(OMe)_3$

The reaction of IrCl(SiNP)(cod) (**5**) with $P(OMe)_3$ (1 : 1 molar ratio) results in the ready formation of the thermally unstable cation 2^+, as well (Scheme 5). However, after approximately 1 h at room temperature, a mixture of **5**, $[IrH(SiNP\text{-}H)\{P(OMe)_3\}_2]^+$ (3^+), and $IrHCl(SiNP\text{-}H)\{P(OMe)_3\}^+$ (**6**) is obtained (^{31}P) with a molar ratio $3^+ : 5 : 6$ = 1.0 : 1.0 : 1.6 (Scheme 5, path A, *cf.* ESI-Fig. S4–S6‡). On the other hand, when the $P(OMe)_3$: **5** molar ratio is ≥2 (Scheme 5, path B) the final mixture of products only contains 3^+, **6** (approx. 1.0 : 1.6) and unreacted $P(OMe)_3$ (^{31}P). Further, once 3^+ and **6** have formed, the molar ratio does not change even if either $P(OMe)_3$ or chloride (as the bis(triphenylphosphane)iminium salt) are added. On this basis, the transformation of 2^+ in either 3^+ or **6** should take place *via* two independent and irreversible paths (*vide infra*).

On the other hand, the final 3^+ : **6** molar ratio does depend on the initial iridium : chloride ratio. Indeed when chloride (as the bis(triphenylphosphane)iminium salt) is added to **5** before adding $P(OMe)_3$ (**5** : PPNCl : $P(OMe)_3$ = 1 : 1 : 2 molar ratio) the 3^+ : **6** molar ratio in the final mixture is approximately 1 : 10.

On a preparative scale, **6** can be separated efficiently from 3^+ by extraction with hexane and it is finally obtained with satisfactory yield as a pure material (*cf.* the Experimental section).

The solution structure of **6** was elucidated by NMR spectroscopy and was found to exhibit the OC-6-43 [6] configuration at the metal centre (Scheme 5). Indeed, the hydride ^1H signal is observed at −9.45 ppm as a doublet-of-triplets ($^2J_{HP}$ = 147.0, 15.5 Hz) indicating that the hydride ligand and the three phosphorus atoms feature a square planar arrangement at the metal center. As a confirmation, the $^{31}P\{^1H\}$ NMR spectrum shows a AXY spin system with $^2J_{PP}$ values confirming the presence of a T-shaped IrP_3 moiety (*cf.* the Experimental section). The coordination sphere of the iridium centre is completed by the chlorido ligand and the methylene group (δ_C = −32.3 ppm). Similar arrangements at iridium(III) have already been described in the solid state.[12]

Like in 3^+, the hydrogen atoms of the $IrCH_2Si$ moiety are non-equivalent (δ_H = 1.15, H^a; 1.22 ppm, H^b, Scheme 5) pointing out the locked conformation of the CH_2–Ir–H fragment in the non-symmetric iridium environment.

The formation of 3^+ and **6** from [2]Cl was monitored by ^{31}P NMR spectroscopy (298 K) but no intermediates could be detected (*cf.* ESI-Fig. S4–S6‡). Thus, given that the transformation of 2^+ into 3^+ and **6** should take place *via* two independent and irreversible reaction paths (*vide supra*) and in view of the reaction pathways shown in Scheme 4, the formation of the square planar complexes $Ir(SiNP)\{P(OMe)_3\}_2^+$ (4^+) and

‖Additionally, based on the difference $\Delta\Delta G^‡$ (2.9 kJ mol^{-1}) between the activation barriers of the C–H oxidative addition in IrCl(SiNP)(CO) and 4^+, a ratio of 3.3 between the corresponding rate constants, $k_4^+/k_{IrCl(SiNP)(CO)} = e^{\Delta\Delta G^‡/RT}$, has been calculated by the Eyring equation. This result fairly matches the fact that the reaction leading to 3^+ is six-fold faster than that leading to IrHCl(SiNP-H)(CO).

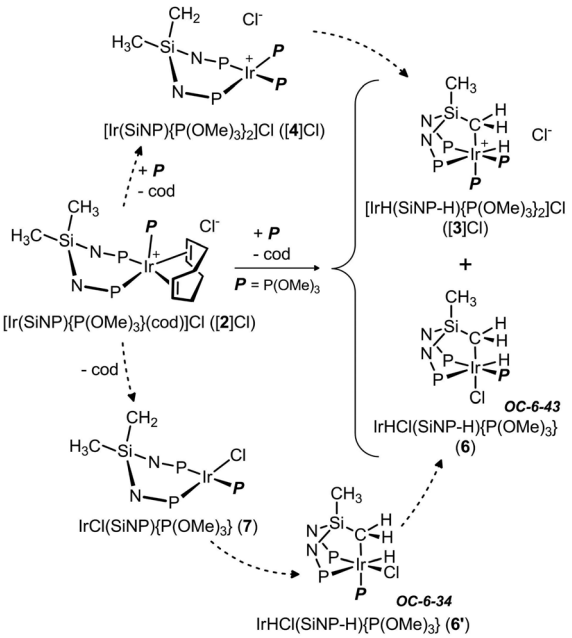

Scheme 6 Proposed mechanism for the formation of [IrH(SiNP-H)-{P(OMe)$_3$}$_2$]Cl ([**3**]Cl) and IrHCl(SiNP-H){P(OMe)$_3$} (**6**) from [Ir(SiNP)-{P(OMe)$_3$}(cod)]Cl ([**2**]Cl).

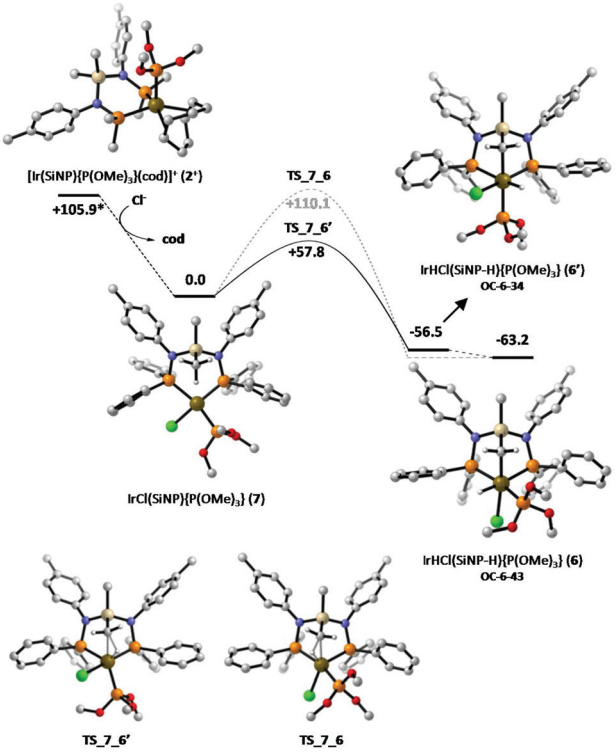

Fig. 6 Energy profile (*G*, kJ mol^{-1}, gas phase, 298 K, 1 atm) for the formation of IrHCl(SiNP-H){P(OMe)$_3$} (**6**) showing the DFT calculated structures of the complexes. *In CH_2Cl_2 (298 K, 1 atm).

IrCl(SiNP){P(OMe)$_3$} (7) could be envisaged as the result of the reactions of **2**$^+$ with P(OMe)$_3$ and chloride ion, respectively (Scheme 6). Consequently **3**$^+$ and **6** should be obtained as the final products after the $SiCH_2$–H oxidative addition to the iridium(I) centre of **4**$^+$ and **7**, respectively (Scheme 6). When dealing with **7**, the solid state structure of square planar complexes of formula IrCl(P-donor)$_3$ has already been described.[13]

As a confirmation, similar to **4**$^+$, the DFT-calculated structure of **7** (Fig. 6) features a boat conformation at the IrP_2N_2Si ring that directs the flag-pole $SiCH_3$ moiety towards the metal centre and makes it susceptible to undergo a concerted C–H oxidative addition. In this respect, it should be noted that when $SiCH_2$–H adds to iridium in **7**, two isomers can be obtained, namely **6** (OC-6-43, chloride *trans* to CH_2) and **6′** (OC-6-34, phosphite *trans* to CH_2) (Scheme 6 and Fig. 6). Nevertheless, only **6** was detected in the course of the reaction (see ESI-Fig. S5–S6‡) and was finally isolated. Accordingly the isomer **6′** was calculated to be 6.7 kJ mol^{-1} less stable than **6**, but, on the other hand, the activation barrier leading to **6′** was calculated to be smaller than that leading to **6**. On this basis, first **6′** should form from **7** and afterwards **6′** should isomerise yielding the more stable OC-6-43 isomer **6** (Scheme 6 and Fig. 6).

Given that the putative intermediate IrCl(SiNP){P(OMe)$_3$} (7) was not directly observed in solution, for the sake of comparison, the rhodium analogue RhCl(SiNP){P(OMe)$_3$} (**8**) was prepared (Scheme 7A).** It is worth mentioning that no oxidative addition of the $SiCH_2$–H bond to rhodium was observed even after refluxing a toluene solution of **8** for 24 h.

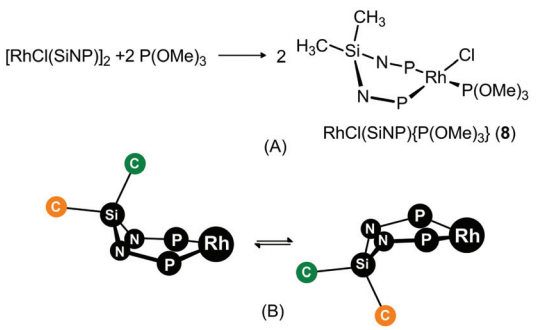

Scheme 7 (A) Synthesis of RhCl(SiNP){P(OMe)$_3$} (**11**). (B) Proposed conformational equilibrium of the RhP_2N_2Ir ring.

The $^{31}P\{^1H\}$ NMR spectrum of **8** shows two non-equivalent SiNP phosphorus atoms occupying two *cis* positions ($^2J_{PP}$ = 39.9 Hz). Consequently, the two tolyl groups are non-equivalent (^1H, ^{13}C, *cf.* the Experimental section). The $^{31}P\{^1H\}$ signal of the coordinated P(OMe)$_3$ moiety is observed at 132.6 ppm as a doublet-of-doublets-of-doublets ($^2J_{PP}$ = 526.1, 49.4 Hz, $^1J_{PRh}$ = 220.3 Hz) in agreement with the proposed T-shaped arrangement of the RhP_3 moiety. Further, the two

In support of the proposed mononuclear structure for **8, it should be noted that its diffusion coefficient is similar to that measured for the mononuclear complex Rh(acac)(SiNP)[2] and the hydrodynamic radius of **8** (5.42 Å) is close to the gyration radius (6.07 Å) of the DFT calculated structure.

SiMe methyl groups are equivalent (^{1}H, ^{13}C) even at 200 K (toluene-d_8) thus pointing out that the up and down semi-spaces at the SiNP ligand should be equivalent or eventually exchange due to a rapid fluxional process. In this respect, it should be noted that the DFT calculated structure of RhCl(SiNP){P(OMe)$_3$} (**8**) features a boat conformation of the RhP_2N_2Si ring. Thus the two $SiMe_2$ methyls are non-equivalent and, reasonably, the rapid inversion of the RhP_2N_2Si ring (Scheme 7B) should be responsible for the observed equivalence of the two $SiMe_2$ methyl groups.

Conclusions

The formation of the Ir^{III}(κ^3*C*,*P*,*P*′–SiNP-H) scaffold takes place *via* the oxidative addition of the $SiCH_2$–H bond to iridium in square planar iridium(I) complexes containing a κ^2*P*,*P*′-coordinated SiNP ligand. Starting from either [Ir(SiNP)(cod)][PF$_6$] ([**1**][PF$_6$]) or IrCl(SiNP)(cod) (**5**), the C–H oxidative addition is triggered by the π-acceptor ligand P(OMe)$_3$. Indeed, with both the iridium complexes, the fluxional and thermally unstable pentacoordinated intermediate [Ir(SiNP){P(OMe)$_3$}(cod)]$^+$ (**2**$^+$) firstly forms. Nevertheless the outcome of the reaction depends on the nature of the counterion of **2**$^+$, namely chloride or hexafluorophosphate.

When the counterion is the non-coordinating anion hexafluorophosphate, **2**$^+$ further reacts with P(OMe)$_3$ eliminating the cod ligand and affording the putative square planar complex [Ir(SiNP){P(OMe)$_3$}$_2$]$^+$ (**4**$^+$). This species exhibits a boat conformation of the IrP_2N_2Si six membered ring, which directs the flag-pole $SiCH_3$ group towards the iridium atom and makes it susceptible to undergo a concerted C–H oxidative addition. As a result the hydride complex [IrH(SiNP-H){P(OMe)$_3$}$_2$]$^+$ (**3**$^+$) is obtained.

On the other hand, when the chloride ion is present in solution, **2**$^+$ affords a mixture of [IrH(SiNP-H){P(OMe)$_3$}$_2$]$^+$ (**3**$^+$) and IrHCl(SiNP-H){P(OMe)$_3$} (**6**). Indeed, besides the reaction of **2**$^+$ with P(OMe)$_3$ affording **3**$^+$, a parallel reaction between **2**$^+$ and chloride takes place yielding the putative square planar intermediate IrCl(SiNP){P(OMe)$_3$} (**7**). Similar to **4**$^+$, the boat conformation of the IrP_2N_2Si ring in **7** directs one $SiCH_3$ moiety towards iridium making this moiety undergo the C–H oxidative addition to the metal.

For both [IrH(SiNP-H){P(OMe)$_3$}$_2$]$^+$ (**3**$^+$) and IrHCl(SiNP-H){P(OMe)$_3$} (**6**) the CH_2–Ir–H moiety is stable in solution and features a locked conformation similar to that observed in the solid state structure of [IrH(SiNP-H){P(OMe)$_3$}$_2$][PF$_6$] ([**3**][PF$_6$]).

Experimental

General section

All the operations were carried out using standard Schlenk-tube techniques under an atmosphere of prepurified argon or in a Braun glove-box under dinitrogen or argon. The solvent was dried and purified according to standard procedures. Bis(triphenylphosphane)iminium chloride (PPNCl, Aldrich) and trimethyl phosphite (P(OMe)$_3$, Aldrich) were commercially available and were used as received. The compounds [IrCl(SiNP)(cod)][PF$_6$][3] ([**1**][PF$_6$]), IrCl(SiNP)(cod)[3] (**5**) and [RhCl(SiNP)]$_2$ [2] were prepared as previously described. NMR spectra were recorded with Bruker spectrometers (AV300 and AV400) and are referred to $SiMe_4$ (^{1}H, ^{13}C) and H_3PO_4 (^{31}P). The ^{13}C NMR signals were assigned according to the ^{1}H–^{13}C HSQC (non-quaternary carbon atoms) and ^{1}H–^{13}C HMBC spectra (quaternary carbon atoms). For clarity the ^{13}C chemical shift (δ_C) of non-quaternary carbon atoms are given along with the ^{1}H NMR data and those of the quaternary atoms afterwards. When dealing with quaternary carbon atoms, it should be noted that only the signals of the C^1 and C^4 atoms of the tolyl groups have been observed in the ^{13}C{^{1}H} NMR spectra and could be assigned reliably. The diffusion experiments were performed using the stimulated echo pulse sequence without spinning and the collected data were treated as previously described.[14] The hydrodynamic radius (R_h) was calculated using the equation of Stokes–Einstein for a spherical diffusing species[14] and the radius of gyration (R_g) was calculated according to the literature,[15] using DFT calculated molecular structures. Elemental analyses were performed by using a Perkin-Elmer 2400 microanalyzer.

Formation of [Ir(SiNP)(cod){P(OMe)$_3$}][PF$_6$] ([2][PF$_6$]). A deep orange solution of [Ir(SiNP)(cod)][PF$_6$] (18.0 mg, 16.6 μmol, 1084.17 g mol^{-1}) and CD_2Cl_2 (0.5 mL) was prepared in a standard 5 mm NMR tube. The solution was cooled at about 243 K and added with P(OMe)$_3$ (2.0 μL, 17 μmol, 124.08 g mol^{-1}, 1.052 g mL^{-1}). As soon as the P(OMe)$_3$ mixed, the solution readily turned pale yellow and the NMR tube was transferred to the NMR spectrometer already equilibrated at 243 K. The solution only contained the new compound [Ir(SiNP)(cod){P(OMe)$_3$}][PF$_6$] ([**2**][PF$_6$]) which was fully characterized *in situ* by NMR spectroscopy. ^{1}H NMR (CD_2Cl_2, 243 K):†† δ = 7.57–7.19 (20H, PPh, δ_C = 133.8, 134.4, *o*-PPh, 127.0, 127.4, *m*-PPh, 130.7, 130.3, *p*-PPh), 6.78 (d, 2H, $^3J_{HH}$ = 8.3 Hz, C^{3}H^{tol,d}, δ_C = 129.0), 6.72 (d, 2H, $^3J_{HH}$ = 8.3 Hz, C^{2}H^{tol,d}, δ_C = 130.4), 6.62 (d, 2H, $^3J_{HH}$ = 8.0 Hz, C^{3}H^{tol,u}, δ_C = 128.8), 6.17 (d, 2H, $^3J_{HH}$ = 8.0 Hz, C^{2}H^{tol,u}, δ_C = 131.7), 3.87 (d, 9H, $^3J_{HP}$ = 10.4 Hz, P(OMe)$_3$, δ_C = 54.8), 3.34 (br, 4H, C$^{sp^2}$H^{cod}, δ_C not observed), 2.34 (br, 4H, C$^{sp^3}$*H*^{endo}H^{exo}, δ_C = 32.4), 2.12 (s, 6H, CH$_3^{tol}$, δ_C = 20.6), 1.92 (br, 4H, C$^{sp^3}$H^{endo}*H*^{exo}), 0.88 (s, 3H, SiC^{u}H$_3$, δ_C = 3.3), −0.50 (s, 3H, SiC^{d}H$_3$, δ_C = 4.0). ^{13}C{^{1}H} NMR (CD_2Cl_2, 243 K): δ = 140.0 (C$^{1,\ tol\text{-}P2}$), 139.7 (C$^{1,\ tol\text{-}P1}$), 136.7 (C$^{4,\ tol\text{-}P2}$), 135.9 (C$^{4,\ tol\text{-}P1}$). ^{31}P{^{1}H} NMR (CD_2Cl_2, 243 K): δ = 87.3 (t, 1P, $^2J_{PP}$ = 14.8 Hz, P(OMe)$_3$), 41.3 (d, 2P, $^2J_{PP}$ = 14.8 Hz, SiNP), −144.7 (sp, 1P, $^1J_{PF}$ = 711.2 Hz, PF_6^-).

Synthesis of [IrH(SiNP-H){P(OMe)$_3$}$_2$][PF$_6$] ([3][PF$_6$]). A dichloromethane solution (5 mL) of [Ir(SiNP)(cod)][PF$_6$] (130 mg, 0.120 mmol, 1084.17 g mol^{-1}) was added with

†† The coordinated P(OMe)$_3$ is supposed to be in the up semispace of the SiNP ligand and the superscript d, down, and u, up, are used accordingly, Fig. 2A.

$P(OMe)_3$ (29.0 μL, mmol, 246 μmol, 124.08 g mol^{-1}, 1.052 g mL^{-1}). The almost colourless resulting solution was stirred for 12 h, partially evaporated and added with hexane, affording a colourless solid which was filtered off, dried *in vacuo* and finally identified as $[IrH(SiNP\text{-}H)\{P(OMe)_3\}_2][PF_6]$ ([**3**][PF_6], 120 mg, 82% yield). Found: C, 45.20; H, 4.77; N, 2.33. Calcd for $C_{46}H_{58}F_6IrN_2O_6P_5Si$ (1224.14): C, 45.13; H, 4.78; N, 2.29. ^1H NMR ($CDCl_3$, 298 K):‡‡ δ = 7.72 (m, 2H, *o*-P^1Ph, δ_C = 134.2), 7.65 (m, 2H, *o*-P^1Ph, δ_C = 134.6), 7.53–7.30 (12H tot: 2H, *o*-P^2Ph, δ_C = 132.2; 4H, *p*-PPh, δ_C = 131.2, 131.1, 130.4, 129.7, 6H, *m*-PPh, δ_C = 127.8, 126.83, 126.77 Hz), 7.04 (m, 2H, *o*-P^2Ph, δ_C = 126.4), 6.90–6.87 (4H tot: 2H, $C^3H^{tol\text{-}P2}$, δ_C = 129.1; 2H, *m*-PPh, δ_C not observed), 6.69 (d, 2H, $^3J_{HH}$ = 7.8 Hz, $C^2H^{tol\text{-}P2}$, δ_C = 129.9), 6.62 (d, 2H, $^3J_{HH}$ = 7.8 Hz, $C^3H^{tol\text{-}P1}$, δ_C = 128.67), 6.15 (d, 2H, $^3J_{HH}$ = 7.8 Hz, $C^2H^{tol\text{-}P1}$, δ_C = 128.65), 3.41 (d, 9H, $^3J_{HP}$ = 17.0 Hz, P^3OCH_3, δ_C = 53.0), 3.38 (d, 9H, $^3J_{HP}$ = 17.1 Hz, P^4OCH_3, δ_C = 52.8), 2.24 (s, 3H, $CH_3^{tol\text{-}P2}$, δ_C = 20.7), 2.08 (s, 3H, $CH_3^{tol\text{-}P1}$, δ_C = 20.4), 0.68 (dq, 1H, $^2J_{HH}$ = 12.3, $^2J_{HP}$ = 10.8, $SiCH^aH^bIr$, δ_C = −26.2, $^2J_{CPtrans}$ = 64.6 Hz, d), 0.36 (dtd, 1H, $^2J_{HH}$ = 12.3, $^2J_{HP}$ = 11.7, $^2J_{HH}$ = 2.4 Hz, $SiCH^aH^bIr$), −0.11 (s, 3H, $SiCH_3$, δ_C = −0.03), −12.0 (dq, 1H, $^2J_{HPtrans}$ = 128.2 Hz, $^2J_{HPcis}$ = 18.0 Hz, Ir–H). $^{13}C\{^1H\}$ NMR ($CDCl_3$, 298 K): δ = 139.2 ($C^{1,\ tol\text{-}P2}$), 139.1 ($C^{1,\ tol\text{-}P1}$), 135.2 ($C^{4,\ tol\text{-}P2}$), 134.2 ($C^{4,\ tol\text{-}P1}$). $^{31}P\{^1H\}$ NMR ($CDCl_3$, 298 K): δ = 89.7 (ddd, 1P, $^2J_{PPcis}$ = 42.1, 23.5, 19.9 Hz, $P^4(OMe)_3$), 73.0 (ddd, 1P, $^2J_{PPtrans}$ = 519.2 Hz, $^2J_{PPcis}$ = 41.9, 21.2 Hz, $P^3(OMe)_3$), 39.1 (dt, 1P, $^2J_{PPtrans}$ = 519.2 Hz, $^2J_{PPcis}$ = 23.8 Hz, $P^{1\text{-}SiNP}$), 38.2 (dt, $^2J_{PPcis}$ = 23.8, 20.9 Hz, 1P, $P^{2\text{-}SiNP}$), −144.4 (sp, 1P, $^1J_{PF}$ = 711.8 Hz, PF_6^-). $D = 6.88 \times 10^{-10}$ m^2 s^{-1} ($CDCl_3$, 298 K), R_h = 5.56 Å, R_g = 6.10 Å.

Synthesis of IrHCl(SiNP-H){P(OMe)$_3$} (6). A CH_2Cl_2 solution (5 mL) of IrCl(SiNP)(cod) (105.0 mg, 0.1077 mmol, 974.66 g mol^{-1}) was added with PPNCl (61.5 mg, 0.107 mmol, 574.04 g mol^{-1}) and then with $P(OMe)_3$ (32 μL, 0.27 mmol, 124.08 g mol^{-1}, 1.052 g mL^{-1}) affording a pale yellow solution. After 3 h stirring all the volatiles were removed *in vacuo* and the residue was extracted with hexane (3 × 10 mL). The hexane extracts were combined and evaporated to dryness, and the resulting pale yellow solid was identified as IrHCl(SiNP-H){$P(OMe)_3$} (**6**, 72.8 mg, 68% yield). When no PPNCl was added, IrHCl(SiNP-H){$P(OMe)_3$} (**6**) was obtained after the same workup with a 45% yield. Found: C, 52.50; H, 5.35; N, 2.45. Calcd for $C_{43}H_{49}ClIrN_2O_3P_3Si$ (990.55): C, 52.14; H, 4.99; N, 2.83. ^1H NMR (C_6D_6, 298 K):‡‡ δ = 8.33–8.20 (4H, *o*-P^1Ph, δ_C = 134.2, 135.3), 7.85 (m, 2H, *o*-P^2Ph, δ_C = 136.8), 7.63 (m, 2H, *o*-P^2Ph, δ_C = 132.7), 7.19–7.10 (10H, *p*-PPh and *m*-P^1Ph), 6.94 (m, 2H, *m*-P^2Ph, δ_C = 126.8), 7.26 (d, 2H, $^3J_{HH}$ = 7.9 Hz, $C^2H^{tol\text{-}P2}$, δ_C = 128.1), 6.90 (d, 2H, $^3J_{HH}$ = 7.9 Hz, $C^3H^{tol\text{-}P2}$, δ_C = 126.8), 6.75 (d, 2H, $^3J_{HH}$ = 7.8 Hz, $C^2H^{tol\text{-}P1}$, δ_C = 130.1), 6.67 (d, 2H, $^3J_{HH}$ = 7.8 Hz, $C^3H^{tol\text{-}P1}$, δ_C = 129.1), 3.63 (d, 9H, $^2J_{HP}$ = 11.3 Hz, POMe, δ_C = 52.5), 1.22 (m, 1H, $^2J_{HH}$ = 12.4, $SiCH^aH^bIr$, δ_C = −32.3), 1.15 (m, 1H, $^2J_{HH}$ = 12.4 Hz, $SiCH^aH^bIr$), 0.10 (s, 3H, $SiCH_3$, δ_C = −0.5), −9.45 (dt, 1H, $^2J_{HP}$ = 147.0, 15.5 Hz, IrH). $^{13}C\{^1H\}$ NMR (C_6D_6, 298 K): δ = 140.0 ($C^{1,\ tol\text{-}P2}$), 139.7 ($C^{1,\ tol\text{-}P1}$), 136.7 ($C^{4,\ tol\text{-}P2}$), 135.9 ($C^{4,\ tol\text{-}P1}$). ^{31}P NMR (C_6D_6, 298 K): 94.1 (dd, 1P, $^2J_{PP}$ = 562.6, 21.7 Hz, $P(OMe)_3$), 46.5 (dd, 1P, $^2J_{PP}$ = 562.6, 21.7 Hz, $P^{1\text{-}SiNP}$), 32.0 (t, 1P, $^2J_{PP}$ = 21.7, $P^{2\text{-}SiNP}$). D = 6.99 × 10^{-10} m^2 s^{-1} ($CDCl_3$, 298 K), R_h = 5.48 Å, R_g = 6.06 Å.

Synthesis of RhCl(SiNP){P(OMe)$_3$} (8). A toluene suspension (5 mL) of $[RhCl(SiNP)]_2$ (68.5 mg, 44.1 μmol, 1554.32 g mol^{-1}) was treated with $P(OMe)_3$ (10.5 μL, 89.0 μmol, 124.08 g mol^{-1}, 1.052 g mL^{-1}). After 30 min stirring, the resulting deep orange solution was partially evaporated (approx. 2 mL left) and added with hexane (5 mL). The resulting suspension was filtered affording a deep orange solid which was dried under vacuum and identified as RhCl(SiNP){$P(OMe)_3$} (**8**, 67.5 mg, 85%). Found: C, 57.44; H, 5.55; N, 3.02. Calcd for $C_{43}H_{49}ClN_2O_3P_3RhSi$ (901.24): C, 57.31; H, 5.48; N, 3.11. ^1H NMR (C_6D_6, 298 K):‡‡ δ = 8.20 (m, 2H, *o*-P^1Ph, δ_C = 135.2), 8.04 (m, 2H, *o*-P^2Ph, δ_C = 134.6), 7.30–7.16 (6H tot: 4H, *m*-PPh, δ_C = 126.9, *m*-P^1Ph; 126.4, *m*-P^2Ph; 2H, *p*-PPh, 128.9, *p*-PPh; 128.2, *p*-PPh), 6.76 (d, 2H, $^3J_{HH}$ = 8.2 Hz, $C^2H^{tol\text{-}P1}$, δ_C = 130.8), 6.73 (s, 4H, $C^2H^{tol\text{-}P2}$ and $C^3H^{tol\text{-}P2}$, δ_C = 131.6, $C^2H^{tol\text{-}P2}$; 128.7, $C^3H^{tol\text{-}P2}$), 6.68 (d, 2H, $^3J_{HH}$ = 8.2 Hz, δ_C = 129.0), 3.46 (d, 9H, $^3J_{HP}$ = 11.7 Hz, $POCH_3$, δ_C = 51.2), 2.03 (s, 3H, $CH_3^{tol\text{-}P1}$, δ_C = 20.4), 2.00 (s, 3H, $CH_3^{tol\text{-}P2}$, δ_C = 20.5), 0.65 (s, 6H, $SiCH_3$, δ_C = 2.8). $^{31}P\{^1H\}$ NMR (C_6D_6, 298 K): δ = 132.6 (ddd, 1P, $^2J_{PPcis}$ = 49.4; $^1J_{PRh}$ = 220.3; $^2J_{PPtrans}$ = 526.1, $P(OMe)_3$), 86.8 (ddd, 1P, $^2J_{PPcis}$ = 39.9; $^2J_{PPcis}$ = 49.4; $^1J_{PRh}$ = 190.8, $P^{2\text{-}SiNP}$), 72.0 (ddd, 1P, $^2J_{PPcis}$ = 39.9; $^1J_{PRh}$ = 134.1; $^2J_{PPtrans}$ = 526.1, $P^{1\text{-}SiNP}$). D = 5.83 × 10^{-10} m^2 s^{-1} (C_6D_6, 298 K), R_h = 5.42 Å, R_g = 6.07 Å.

Solid state structure determination of [IrH(SiNP-H){P(OMe)$_3$}$_2$][PF$_6$] ([3][PF$_6$]). Single crystals of $[IrH(SiNP\text{-}H)\{P(OMe)_3\}_2][PF_6]$ ([**3**][PF_6]) suitable for a X-ray diffraction study were obtained by slow diffusion of diethylether into a CH_2Cl_2 solution of the compound. The intensities were collected at 100 K using a Bruker SMART APEX diffractometer with graphite-monochromated Mo Kα radiation (λ = 0.71073 Å) following standard procedures. The intensities were integrated and corrected for absorption effects using the SAINT+[16] and SADABS[17] programs, included in the APEX2 package. The structure was solved by Patterson's method. All non-hydrogen atoms were located in the subsequent Fourier maps. Refinement was carried out by full-matrix least-squares procedure (based on F_o^2) using anisotropic temperature factors for all non-hydrogen atoms. The C–H hydrogen atoms were placed in calculated positions with fixed isotropic thermal parameters (1.2 × U_{equiv}) of the parent carbon atom. The coordinates of the Ir–H hydrogen atom were calculated using the XHYDEX[18] program implemented in the WinGX[19] package and the hydrogen was finally refined using restraints (DFIX). Calculations were performed with SHELX-97[20] program implemented in the WinGX package.[19]

Crystal data for $[IrH(SiNP\text{-}H)\{P(OMe)_3\}_2][PF_6]\cdot Et_2O$, [**7**][$PF_6$]·$Et_2O$: $C_{46}H_{58}F_6IrN_2O_6P_5Si\cdot C_4H_{10}O$, M = 1298.20 g mol^{-1}; colorless prism, 0.30 × 0.20 × 0.06 mm; monoclinic, $P2_1/n$; a = 11.9408(9) Å, b = 31.183(2) Å, c = 14.8638(11) Å, β = 93.5760(10)°; Z = 4; V = 5523(7) Å^3; D_{calc} = 1.561 g cm^{-3}; μ = 2.654 mm^{-1}, T_{min} = 0.628; T_{max} = 0.853; 79 012 collected reflec-

‡‡The superscript tol-P*X* is used to designate the tolyl group of the P^X-*N*-tolyl moiety.

tions ($1.306° \leq \theta \leq 27.998°$), 13 146 unique ($R_{int}$ = 0.0548); 13 146/6/662 data/restraints/parameters; GOF = 1.049; R_1 = 0.0354 ($I > 2\sigma(I)$), 0.0513 (all data); wR_2 = 0.0787 ($I > 2\sigma(I)$), 0.0872 (all data).

CCDC deposit number 1413967.

DFT geometry optimization

The molecular structures were optimized at the DFT-BP3LYP level (298 K, 1 atm) using the Gaussian09 program.[21] The LanL2TZ(f) basis[22] and pseudo-potential were used for rhodium and iridium and the 6-31G(d,p) basis set for the remaining atoms. Stationary points were characterised by vibrational analysis (one imaginary frequency for transition states, only positive frequencies for minimum energy molecular structures). All the structures were optimized in the gas phase and in selected cases also in CH_2Cl_2 using the CPCM method. The NMR data were calculated using the GIAO method in CH_2Cl_2 (CPCM method) and the atomic charge at iridium in IrCl(SiNP)(CO) and Ir(SiNP)$\{P(OMe)_3\}_2]^+$ ($\mathbf{4}^+$) was obtained from the Hirshfeld population analysis.

Abbreviations

cod	1,5-Cyclooctadiene
SiNP	$SiMe_2\{N(4\text{-}C_6H_4CH_3)PPh_2\}_2$
SiNP-H	$Si(CH_2)(CH_3)\{N(4\text{-}C_6H_4CH_3)PPh_2\}_2$

Acknowledgements

Financial support from Spanish "Ministerio de Economía y Competitividad" (CTQ2013-42532-P), "Diputación General de Aragón" (Group E07) and University of Zaragoza (UZCUD2014-CIE-13) is gratefully acknowledged.

Notes and references

1 (*a*) E. Carter, K. Cavell, W. F. Gabrielli, M. J. Hanton, A. J. Hallett, L. McDyre, J. A. Platts, D. M. Smith and D. M. Murphy, *Organometallics*, 2013, **32**, 1924; (*b*) N. Cloete, H. G. Visser, I. Engelbrecht, M. J. Overett, W. F. Gabrielli and A. Roodt, *Inorg. Chem.*, 2013, **52**, 2268; (*c*) T. Mayer and H.-C. Boettcher, *Polyhedron*, 2013, **50**, 507; (*d*) T. Ogawa, Y. Kajita, Y. Wasada-Tsutsui, H. Wasada and H. Masuda, *Inorg. Chem.*, 2013, **52**, 182; (*e*) I. Pernik, J. F. Hooper, A. B. Chaplin, A. S. Weller and M. C. Willis, *ACS Catal.*, 2012, **2**, 2779; (*f*) S. Todisco, V. Gallo, P. Mastrorilli, M. Latronico, N. Re, F. Creati and P. Braunstein, *Inorg. Chem.*, 2012, **51**, 11549; (*g*) L. H. Do, J. A. Labinger and J. E. Bercaw, *Organometallics*, 2012, **31**, 5143; (*h*) F. Trentin, A. M. Chapman, A. Scarso, P. Sgarbossa, R. A. Michelin, G. Strukul and D. F. Wass, *Adv. Synth. Catal.*, 2012, **354**, 1095; (*i*) L. E. Bowen, M. Charernsuk, T. W. Hey, C. L. McMullin, A. G. Orpen and D. F. Wass, *Dalton Trans.*, 2012, **39**, 560; (*j*) B. Aluri, N. Peulecke, B. H. Muller, S. Peitz, A. Spannenberg, M. Hapke and U. Rosenthal, *Organometallics*, 2012, **29**, 226; (*k*) H. W. Cheung, C. M. So, K. H. Pun, Z. Zhou and C. P. Lau, *Adv. Synth. Catal.*, 2011, **353**, 411; (*l*) J. Gopalakrishnan, *Appl. Organomet. Chem.*, 2009, **23**, 291; (*m*) O. V. Ozerov, C. Guo and B. M. Foxman, *J. Organomet. Chem.*, 2006, **691**, 4802; (*n*) A. Bollmann, K. Blann, J. T. Dixon, F. M. Hess, E. Killian, H. Maumel, D. S. McGuiness, D. H. Morgan, A. Neveling, S. Otto, M. Overett, A. M. Z. Slawin, P. Wasserscheid and S. Kuhlmann, *J. Am. Chem. Soc.*, 2004, **126**, 14712; (*o*) A. M. Z. Slawin, M. Wainwright and J. D. Woolins, *J. Chem. Soc., Dalton Trans.*, 2002, 513.

2 V. Passarelli and F. Benetollo, *Inorg. Chem.*, 2011, **50**, 9958.

3 V. Passarelli, J. J. Pérez–Torrente and L. A. Oro, *Inorg. Chem.*, 2014, **53**, 972.

4 M. Albrecht, *Chem. Rev.*, 2010, **110**, 576.

5 (*a*) A. Sundermann, O. Uzan, D. Milstein and J. M. L. Martin, *J. Am. Chem. Soc.*, 2000, **122**, 7095; (*b*) B. Rybtchinski and D. Milstein, *J. Am. Chem. Soc.*, 1999, **121**, 4528; (*c*) M. E. van der Boom, S.-Y. Liou, Y. Ben–David, M. Gozin and D. Milstein, *J. Am. Chem. Soc.*, 1998, **120**, 13415; (*d*) B. Rybtchinski, A. Vigalok, Y. Ben-David and D. Milstein, *J. Am. Chem. Soc.*, 1996, **118**, 12406.

6 *Nomenclature of Inorganic Chemistry. IUPAC Recommendations 2005*, ed. N. G. Connely and T. Damhus, Royal Society of Chemistry, Cambridge, 2005.

7 (*a*) J. F. Frazier and J. S. Merola, *Polyhedron*, 1992, **11**, 2917; (*b*) D. A. Krogstad, A. J. De Boer, W. J. Ortmeier, J. W. Rudolf and J. A. Halfen, *Inorg. Chem. Commun.*, 2005, **8**, 1141.

8 (*a*) A. M. Gull, P. E. Fanwick and C. P. Kubiak, *Organometallics*, 1993, **12**, 2121; (*b*) X. Sava, N. Mezailles, L. Ricard, F. Mathey and P. Le Floch, *Organometallics*, 1999, **18**, 807.

9 (*a*) D. L. Thorn and T. H. Tulip, *Organometallics*, 1982, **1**, 1580; (*b*) J. D. Feldman, J. C. Peters and T. D. Tilley, *Organometallics*, 2002, **21**, 4050; (*c*) L. Dahlenburg and R. Hache, *Inorg. Chim. Acta*, 2003, **350**, 77; (*d*) Y. Gloaguen, L. M. Jongens, J. N. H. Reek, M. Lutz, B. De Bruin and J. I. Van der Vlugt, *Organometallics*, 2013, **32**, 4284.

10 (*a*) G. R. Clark, B. W. Skelton and T. N. Waters, *J. Organomet. Chem.*, 1975, **85**, 375; (*b*) G. R. Clark, B. W. Skelton, T. N. Waters and J. E. Davies, *Acta Crystallogr., Sect. C: Cryst. Struct. Commun.*, 1987, **43**, 1708; (*c*) O. Blum, J. C. Calabrese, F. Frolow and D. Milstein, *Inorg. Chim. Acta*, 1990, **174**, 149; (*d*) U. Casellato, B. Corain, R. Graziani, B. Longato and G. Pilloni, *Inorg. Chem.*, 1990, **29**, 1193; (*e*) S. S. Oster and W. D. Jones, *Polyhedron*, 2004, **23**, 2959; (*f*) M. G. Crestani, A. Steffen, A. M. Kenwright, A. S. Batsanov, J. A. K. Howard and T. B. Marder, *Organometallics*, 2009, **28**, 2904; (*g*) J. Langer, W. Imhof, M. J. Fabra, P. Garcia-Orduna, H. Gorls, F. J. Lahoz, L. A. Oro and M. Westerhausen, *Organometallics*, 2010, **29**, 1642; (*h*) M. J. Geier, C. M. Vogels, A. Decken and S. A. Westcott, *Eur. J. Inorg. Chem.*, 2010, 4602.

11 C. A. Tolman, *Chem. Rev.*, 1977, **77**, 313.

12 (*a*) D. Milstein and J. C. Calabrese, *J. Am. Chem. Soc.*, 1982, **104**, 3773; (*b*) D. Milstein, W. C. Fultz and J. C. Calabrese, *J. Am. Chem. Soc.*, 1986, **108**, 1336; (*c*) H. E. Selnau and J. S. Merola, *Organometallics*, 1993, **12**, 1583; (*d*) M. Ciclosi, F. Estevan, P. Lahuerta, V. Passarelli, J. Perez-Prieto and M. Sanau, *Adv. Synth. Catal.*, 2008, **350**, 234.

13 (*a*) L. Hintermann, M. Perseghini, P. Barbaro and A. Togni, *Eur. J. Inorg. Chem.*, 2003, 601; (*b*) R. S. Simons, M. J. Panzner, C. A. Tessier and W. J. Youngs, *J. Organomet. Chem.*, 2003, **681**, 1; (*c*) A. G. Orpen, P. G. Pringle, M. B. Smith and K. Worboys, *J. Organomet. Chem.*, 1998, **550**, 255; (*d*) K. Tani, K. Nakajima, A. Iseki and T. Yamagata, *Chem. Commun.*, 2001, 1630; (*e*) J. Goodman, V. V. Grushin, R. B. Larichev, S. A. Macgregor, W. J. Marshall and D. C. Roe, *J. Am. Chem. Soc.*, 2010, **132**, 12013; (*f*) H.-C. Bottcher, M. Graf and K. Merzweiler, *Polyhedron*, 1997, **16**, 341.

14 (*a*) P. Stilbs, *Prog. Nucl. Magn. Reson. Spectrosc.*, 1987, **19**, 1; (*b*) W. S. Price, *Concepts Magn. Reson.*, 1997, **9**, 299; (*c*) W. S. Price, *Concepts Magn. Reson.*, 1998, **10**, 197; (*d*) C. S. Johnson Jr., *Prog. Nucl. Magn. Reson. Spectrosc.*, 1999, **34**, 203; (*e*) Y. Cohen, L. Avram and L. Frish, *Angew. Chem., Int. Ed.*, 2005, **117**, 524; (*f*) Y. Cohen, L. Avram and L. Frish, *Angew. Chem., Int. Ed.*, 2005, **44**, 520; (*g*) P. S. Pregosin, P. G. A. Kumar and I. Fernandez, *Chem. Rev.*, 2005, **105**, 2977; (*h*) A. Macchioni, G. Ciancaleoni, C. Zuccaccia and D. Zuccaccia, *Chem. Soc. Rev.*, 2008, **37**, 479.

15 A. Ortega, D. Amorós and J. García de la Torre, *Biophys. J.*, 2011, **101**, 892.

16 *SAINT+, version 6.01*, Bruker AXS, Inc., Madison, WI, 2001.

17 G. M. Sheldrick, *SABADS*, University of Göttingen, Göttingen, Germany, 1999.

18 A. G. Orpen, *J. Chem. Soc., Dalton Trans.*, 1980, 2509.

19 L. J. Farrugia, *J. Appl. Crystallogr.*, 1999, **32**, 837.

20 (*a*) G. M. Sheldrick, *SHELXL-97*, University of Göttingen, Göttingen, Germany, 1997; (*b*) G. M. Sheldrick, *Acta Crystallogr., Sect. A: Fundam. Crystallogr.*, 2008, **64**, 112.

21 M. J. Frisch, *et al.*, *Gaussian 09 (Revision A.02)*, Gaussian, Inc., Wallingford, CT, 2009.

22 (*a*) P. J. Hay and W. R. Wadt, *J. Chem. Phys.*, 1985, **82**, 270; (*b*) W. R. Wadt and P. J. Hay, *Chem. Phys.*, 1985, **82**, 84; (*c*) L. E. Roy, P. J. Hay and R. L. Martin, *J. Chem. Theory Comput.*, 2008, **4**, 1029.

